ALMA Memo 354
Choices of Antenna Size and Number for the Atacama Compact Array

Wm. J. Welch
UC Berkeley

August 25, 2000

Abstract

The lack of large scale structure in array maps is the result of the hole in the center of the visibility plane that arises because the smallest spacing between antennas is limited to one antenna diameter. Visibility data may be extracted for a region in the center of the hole from a single antenna map made with one array antennas. This can be accomplished by Fourier transforming the map and dividing out the transform of the gain function to produce the visibility. If a mosaic of pointings is obtained with the array in its interferometric mode, this data set allows extrapolation of the visibilities inward from the edge of the hole. This can be done by a similar procedure in which the same gain function is divided from the observed visibilities to obtain visibilities within the edge of the hole. From the overlap, a complete map may be constructed. Pointing errors spoil this procedure. The effect of the pointing errors is to produce phase and amplitude errors in the visibilities that increase toward the overlap region from both the origin and the edge of the hole. This is doubly bad, because the transforms of the gain functions also tend toward zero in the overlap region and the data errors are amplified there. For the homogeneous array, the effects of even small errors in pointing are severe. The use of an array of smaller antennas provides a better overlap in the central hole, and reduces the effects of pointing errors. The smaller the compact array antennas, the better is the overlap, but more antennas are required and calibration becomes more difficult. A reasonable compromise would be 6m, half the 12m diameter diameter and a traditional choice. For the compact array to contribute a point source sensitivity that matches that of the more closely spaced 12m antennas, the necessary number of

small antennas is approximately $(12/D_c)\times 6$, where D_c is the diameter of the compact array antenna. As an example, the compact D array of the 10 BIMA antennas shows reasonably good overlap with Kogan's (1998) 12m D array.

1 Introduction

Imaging of fields larger than the primary beam of the 12m ALMA antenna will be important for some of the science that is planned for the system. Whereas this can be accomplished, in principle, with a homogeneous array, simulations which include modest antenna pointing errors show that the dynamic range and fidelity of the maps are considerably degraded by the pointing errors (Cornwell, 1998; Holdaway, private comm., Morita, private comm.). Including a compact array as part of the system will help a great deal with this problem. The present questions are (1) What is the best choice of antenna size for the small array? and (2) How many antennas are needed? The following discussion attempts to provide a frame- work for answering the questions.

2 Effect of Pointing Errors on Mosaic Images with a Homogeneous Array

In principal, imaging of large fields with a homogeneous array is possible through the combination of single dish observations with the array elements and mosaic pointing during interferometric observations with the array. However, pointing errors can have a devastating effect on the accuracy of the results (Cornwell, 1988). To understand how these effects can be mitigated through the use of a small compact array, it is useful to consider how the pointing errors affect the visibility data which produce the maps.

The array produces visibility data for all of the uv plane except for the hole in the center with radius D, the diameter of the array antennas. The antenna pairs cannot be placed closer than one dish diameter. One or more of the elements, operating in single antenna mode, can be used to add data into the hole. The latter data is observed in the image plane, whereas the array data arrives in the visibility plane. The two are linearly related by the Fourier transform. The table bellow lists transform pairs which are useful for the following discussion.

Fourier Transforms	Image plane	Visibility plane
sky brightness	$T_B(x,y)$	V(u,v)
antenna gain	g(x,y)	G(u,v)
antenna temperature	$T_A(x,y)$	$t_A(u,v)$

The image plane is x,y and u,v is the visibility plane. $T_B(x,y)$ is the desired image, V(u,v) is its visibility, and $T_A(x,y)$ is a map of the source made with a single antenna.

To get the needed visibility data in the hole, one first makes a map of the source with one or more of the antennas used in single dish mode and transforms it to visibility data. Second, one obtains data from the array both interferometrically and, at the same time, making multiple pointings of the source, adds it to the array data in the appropriate way, and produces a complete map from the combination.

The single antenna map is $T_A(x,y)$. Since this is a convolution of $T_B(x,y)$ with the antenna gain function, $T_A(x,y)$=$T_B(x,y) * g(x,y)$, it can be transformed to $t_A(u,v)$=V(u,v)G(u,v) in the visibility plane. To extract V(u,v) it is necessary to form effectively the fraction

$$V(u,v) = t_A(u,v)/G(u,v), \tag{1}$$

which works except where where $G \rightarrow 0$. Since g(x,y) is typically close to a Gaussian function, G(u,v) is as well. Let Θ be the FWHM of the antenna with a circular beam and $\theta^2 = x^2 + y^2$.

$$g(\theta) \propto e^{-2.76(\theta/\Theta)^2} \tag{2}$$

Then G(u,v) has a similar form in terms of the radial visibility variable. $\beta = \sqrt{(}u^2 + v^2)$

$$G(\beta) \propto e^{-3.58\Theta^2\beta^2} \tag{3}$$

The connection between Θ and D, the antenna diameter, is the usual diffraction formula.

$$\Theta = 1.2\lambda/D \tag{4}$$

Figure 1 shows the cross-section of the visibility plane near the origin. For single pointing of the array antennas, visibility is measured only for $\beta \geq D/\lambda$. A plot of equation(3) in Figure 1 shows that $G(\beta) \rightarrow 0$ before β reaches D/λ. Thus, visibility data cannot be extracted from the single antenna observations all the way out to $\beta \sim D/\lambda$.

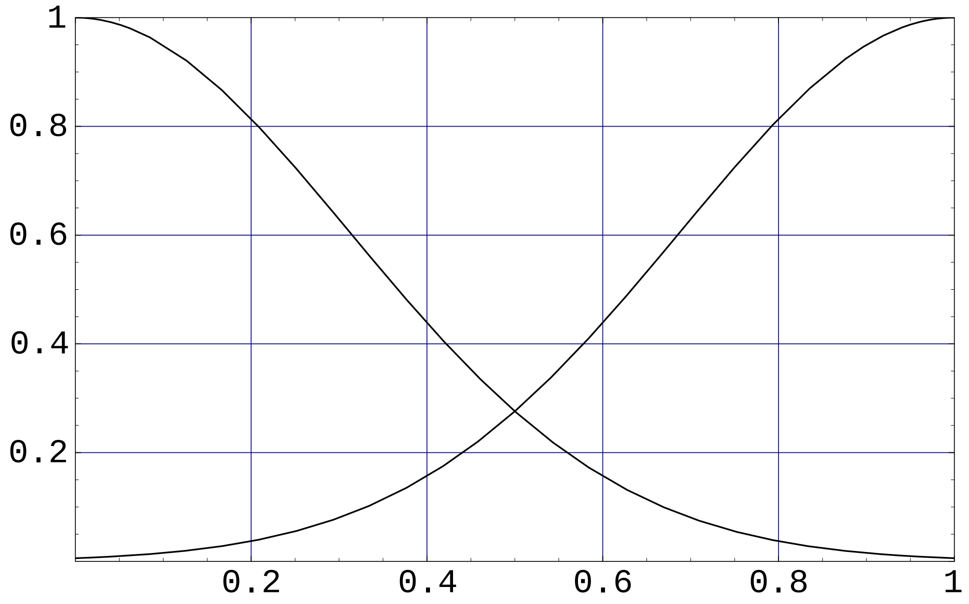

Figure 1: Transfer functions for the homogeneous array. The abscissa is the radial variable in the visibility plane normalized to D/λ, where D is the antenna diameter. The curve on the left is the transform of the antenna gain function. The curve on the right is the function which weights the extrapolation of visibility from the array multipointing observations. It is the same function, except that it is centered at $\beta = D/\lambda$.

Measurement of visibility data within the outer parts of the hole from the array is obtained by doing multiple pointing (mosaicing) of the array antennas while they are observing the source (Ekers, and Rots, 1979; Cornwell, 1988). A transform of this data set made with respect to the mosaic of pointings (x_o, y_o) leads to the following formal result for the measured visibility.

$$G(u_o, v_o)V(u - u_o, v - v_o), \tag{5}$$

where u_o and v_o are the variables in the transform from the mosaic pointings, x_o, y_o. The result is that there are measured visibility data off the ordinary u,v tracks at distances given by u_o, v_o, weighted by $G(u_o, v_o)$. Recovering visibilities from equation (5) requires the same kind of division that is implied by equation (1). Depending on the width of G(u,v), this data will overlap that which comes from the single dish measurements. For the homogeneous array, it is the same G(u,v) for both contributions, and this distribution is shown as another plot of equation (3) centered at the smallest value of β given by the array, D/λ, in Figure 1. The overlap is now significant and shows why the combination of single dish plus mosaic array data for the homogeneous array should give an image that is fully sampled and accurate at the short spacings. Simulations show that it works for perfect data.

The presence of pointing errors spoils the image formation contributions of both the single antenna maps and the array visibility observations. It is useful to consider them separately.

2.1 The Visibility Errors from the Single Antenna

From the single antenna map, visibility data is extracted corresponding to values of u and v from 0 to $\leq D/\lambda$. In this data, the larger values of u and v correspond to greater separations of pairs of patches on the antenna. Figure 2 illustrates how phase errors in these visibilities arise if there are pointing errors. Figure **??** also suggests a way to evaluate the effects of the pointing errors. Begin with the explicit connection between $T_A(x, y)$ and its transform.

$$T_A(x, y) = \int_{-\infty}^{\infty} V(u, v)G(u, v)e^{i2\pi(ux+vy)}dudv \tag{6}$$

With pointing errors δx and δy,

$$T_A(x + \delta x, y + \delta y) = \int_{-\infty}^{\infty} V(u, v)[G(u, v)e^{i2\pi(u\delta x+v\delta y)}]e^{i2\pi(ux+vy)}dudv \tag{7}$$

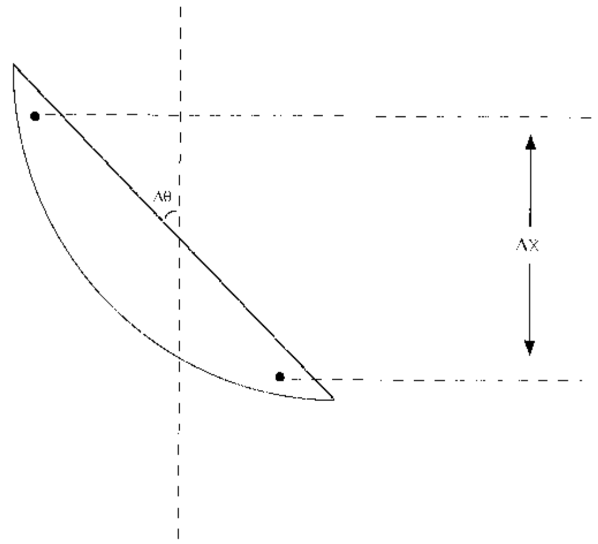

Figure 2: Sketch of an antenna with a pointing error. Lines to two patches on the reflector are shown. Visibilities corresponding to this separation, Δx, suffer a phase error of $(2\pi/\lambda)\Delta x \Delta\theta$.

The effective transfer function is now

$$G_{eff}(u,v) = G(u,v)e^{i2\pi(u\delta x + v\delta y)} \sim G(\beta)e^{i2\pi\beta\delta\theta} \quad (8)$$

G_{eff}(u,v) contains phase errors which will distort the Visibility V(u,v) derived from equation (1). The phase errors are greater for larger u and v for a given pointing error. The use of a radial cut in the uv plane with the radial variable $\beta = \sqrt{(}u^2 + v^2)$ simplifies the discussion.

Consider two limiting cases. In the first, the errors change slowly, perhaps during a snap-shot observation, but are randomly distributed among the antennas with RMS expectation σ_θ. If the pointing error in the phase term of equation(8) is replaced by its expectation and β is set equal to sD/λ, where $0 \le s \le 1$, so that s is the radial variable of the hole normalized to one, then the typical phase error is

$$\Delta\phi = 2\pi\beta\sigma_\theta = 2\pi(sD/\lambda)\sigma_\theta = 2.4\pi s(\sigma_\theta/\Theta) \quad (9)$$

It is at the half radius, s=1/2, where the visibility data from the single dish measurements must overlap with those obtained from the array. For (σ_θ/Θ)=0.1, one tenth beamwidth pointing accuracy, $\Delta\Phi = .38(22^o)$ at this point. For (σ_θ/Θ)=.05, it is $0.19(11^o)$. These are large errors from small pointing errors. Perley (1989) notes that a 10^o phase error is equivalent to a visibility amplitude error of 20% in the construction of images.

In the other limiting case, the pointing errors vary rapidly at each antenna during the observations, perhaps due to the wind. In this case, the phase errors approximately average out to zero. However, there is a loss in amplitude due to the decorrelation caused by the fluctuating phase. If the fluctuations are normally distributed,

$$Expectation[e^{i\phi}] = e^{-\sigma_\phi^2/2} \quad (10)$$

From the discussion above, with σ_θ now corresponding to rapid fluctuations,

$$\sigma_\phi^2 = (2.4\pi s\sigma_\theta/\Theta)^2 \quad (11)$$

and the loss of amplitude is by the following factor.

$$e^{-1/2(2.4\pi s\sigma_\theta/\Theta)^2} \quad (12)$$

At the mid radial point, s=1/2, this factor is 0.93 for σ_θ/Θ=0.1. The functional form of this error factor is a Gaussian just like the basic function $G(\beta)$ in equation (3). Including this factor in equation(3) leads to a narrower and uncertain composite Gaussian. Altogether, the effective overlap region is reduced as well as the visibility data being made uncertain.

2.2 Visibility Errors from Scanning the Array Antennas(Mosaicing)

Equation (5) above is the result of a transform of the visibility data from the array with respect to the mosaic of pointings, x_o, y_o. The effect of the multiple pointings is to provide interferometer visibilities with the set of gain functions $g(x - x_o, y - y_o)$. That is, we get a different interferometric image from each pointing. The effect of pointing errors on these observations can be found starting with the transform of $g(x - x_o, y - y_o)$.

$$g(x - x_o, y - y_o) = \int_{-\infty}^{\infty} G(u, v) e^{i2\pi[u(x-x_o)+v(y-y_o)]} du dv \qquad (13)$$

With pointing errors δx and δy in x_o and y_0 respectively,

$$g(x-x_o-\delta x, y-yo-\delta y) = \int_{-\infty}^{\infty} [G(u, v) e^{-i2\pi(u\delta x+v\delta y)}] e^{i2\pi[u(x-x_o)+(y-y_o)]} du dv \qquad (14)$$

Just as in equation (8) above, the pointing errors in the array give rise to an erroneous effective G_{eff}(u,v) which is G(u,v) with the additional factor $e^{-i2\pi(u\delta x+v\delta y)}$. All the relations worked out above apply in this case as well. Both the phase errors and amplitude errors increase with distance u_o and v_o away from the regular uv track. In particular, the data extrapolation inward from the edge of the hole is more uncertain the farther it is carried.

It is clear how the image fidelity and dynamic range are degraded by the pointing errors for the homogeneous array. Where the two data sets overlap at the half diameter radius of the hole, they spoil the inter-comparison, so that the good mutual calibration of the data sets is degraded. In addition, because the weighting by the gain transfer function at the half radius point is only $\leq .25$ of what it is elsewhere, the errors are multiplied up in the inversion process.

3 The Important Contribution of the Compact Array

The compact array of smaller antennas will ameliorate the problem by providing visibilities in the outer part of the hole in the central visibility plane. The most central visibilities will be provided by maps made by a few of the 12m antennas operating in single antenna mode as above. The array should be chosen for good overlap with the 12m uv coverage. The overlap can be seen in Figure 3 which, like Figure 1, shows a cross-section of the visibility plane. The function G(u,v) for the 12m dish is shown for the central region. Also shown are the multiply pointed array G(u,v) functions in the overlap regions for 4m, 6m, 8m, and 12m antennas. Pointing of the smaller antennas may be better enough that the errors of the 12m will dominate. It is clear that the smaller the antenna in the compact array the better is the overlap and the smaller will be the effect of the 12m pointing errors. Current experience is that if the smaller dishes are 1/2 the diameter of the single dish or smaller, good images are possible. The best results that have been obtained are with the Compact AT and the Parkes telescope operating at the HI line. In this latter case, the ratio of dish diameters is about 3. This would argue in favor of using 4m antennas. The difficulty with this choice is both in the phase calibration and the number of antennas needed for good signal/noise. The 8m antennas will be easier to calibrate but offer poorer overlap in the uv plane. The better overlap of the 6m antenna argues that it may be the best compromise. It may also have smaller fractional pointing errors than the 8m, and that is another advantage.

4 The number of Antennas in the Compact Array

The compact array uv coverage must overlap with that of the inner part of the 12m array and provide adequate sensitivity for the particular part of the uv plane that it occupies. For example, for a 6m array, this part is approximately the annulus that extends from 6m to the 12m inner boundary of the 12m array uv coverage. One approach is to require that the point source sensitivity of the compact array be the same as that of an equal area annulus at the inner edge of the 12m coverage. An example of a compact 12m array uv coverage is that of Kogan's optimum D array (Kogan, 1998) reproduced here as Figure 4. This figure shows both the antenna locations (diamonds) and snap-shot uv points. The number of uv points in the 12m inner edge annulus is about 46 and corresponds to 23 spacings (after correcting for the Hermitian doubling) which is the work of 6.7 12m antennas. The array of smaller antennas should have the same point source sensitivity in its coverage of the inner annulus. For comparison of antenna sensitivity, the important point is that both the small and large antenna arrays are operating in multiple pointing mode here. In the mapping, by multiple pointing, of a given region in a set amount of time the relative sensitivity to any point source in the field is proportional to the antenna diameter, not antenna diameter squared as it is for the single pointing case

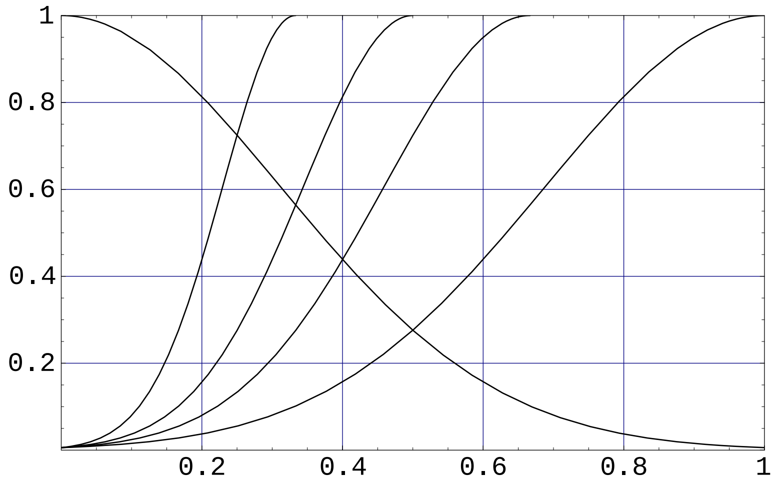

Figure 3: This is the same as Figure 1, except that more curves have been added. In addition to the weighting function for the extrapolation of array visibility data from the 12m antenna, there are weighting function curves for compact arrays of 8m, 6m, and 4m antennas. The curves are shown in that order from right to left. The smaller the array antenna relative to the single antenna, the better the overlap with the visibilities measured with the single antenna.

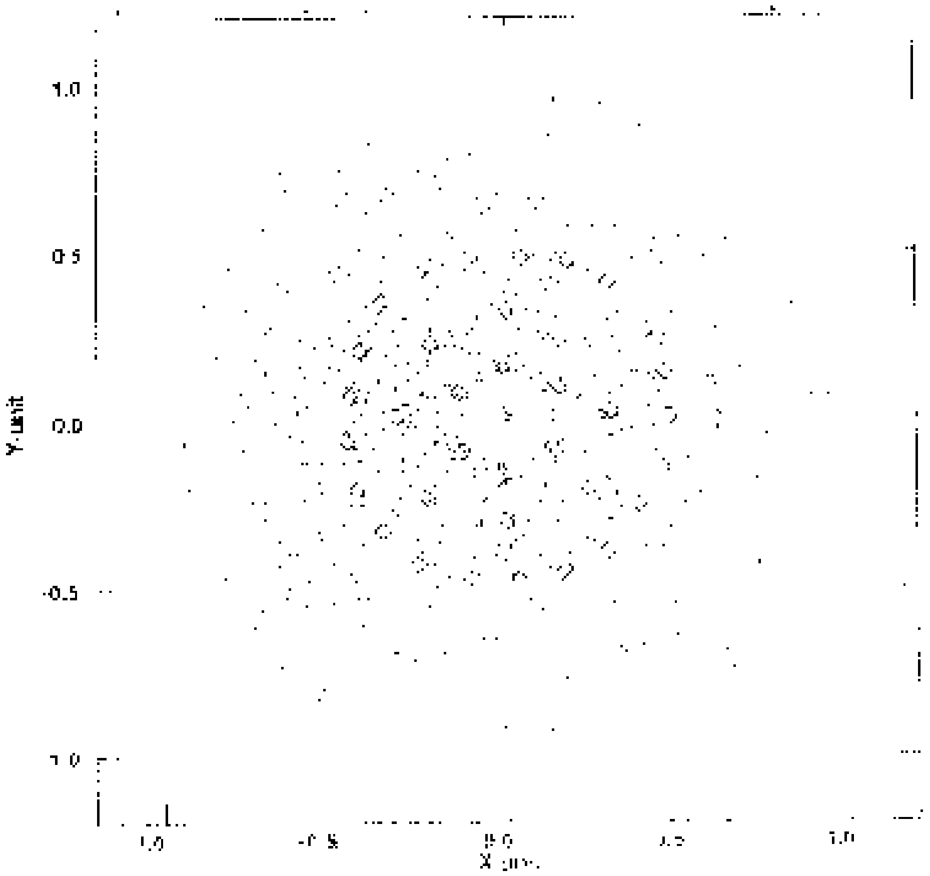

Figure 4: The snapshot uv coverage for Kogan's D array.

(Sargent and Welch, 1993). The number of compact array antennas should be $\approx (12/D_c) \times 6$, where D_c is the diameter of the compact array. Thus, for 6m antennas, 12 - 13 seem to be required. For 4m, the number would be closer to 20, and for 8m 9 or 10 would be required. In fact, requiring the same point source sensitivity may be too strong, since the typical visibility function of a complex field is small over most of the uv plane and grows rapidly near the origin of the uv plane. A smaller number for the inner region may give the same signal/noise. Thus, a sufficient number might be, for example, 10 at 6m for the compact array, for good signal/noise in a complex field.

5 A Straw-person Compact Array, The BIMA D-Array

The compact array of the previous paragraph is close enough to the 10 element BIMA D-Array that it may be of use to describe the latter as a starting point for further discussion. Figure 5 shows the layout of the BIMA D-Array. The smallest separation is 1.35 times the antenna diameter. It is a compromise between small spacings and the problem of shadowing. Foreshortening leads to spacings at one antenna diameter except overhead. This array works well at the Hat Creek latitude of 41^o for declinations above about -10^o, but below that, shadowing makes it rather useless. A similar problem will occur at the Chilean site for high northern declinations, and it may require a small set of rails for reconfiguration for extreme declinations. On the other hand, the ALMA 12m D-Array may work with fewer antennas that are shadowed for the extreme declinations, getting the short spacings by baseline foreshortening. Figure 6 shows the BIMA D-Array uv coverage for a snap-shot. There are 90 uv points, most of them within a radius of 5.4 kλ, corresponding to 16.2m radius for the hole in the uv plane. This number is roughly twice the number of 12m visibility points in the 12m annulus as required for comparable point source sensitivity. 16.2m is 1.35×12m, which is a plausible minimum separation for the 12m antennas to avoid shadowing.

6 Acknowledgement

It is a pleasure to acknowledge helpful discussions with Tam Helfer and Mel Wright.

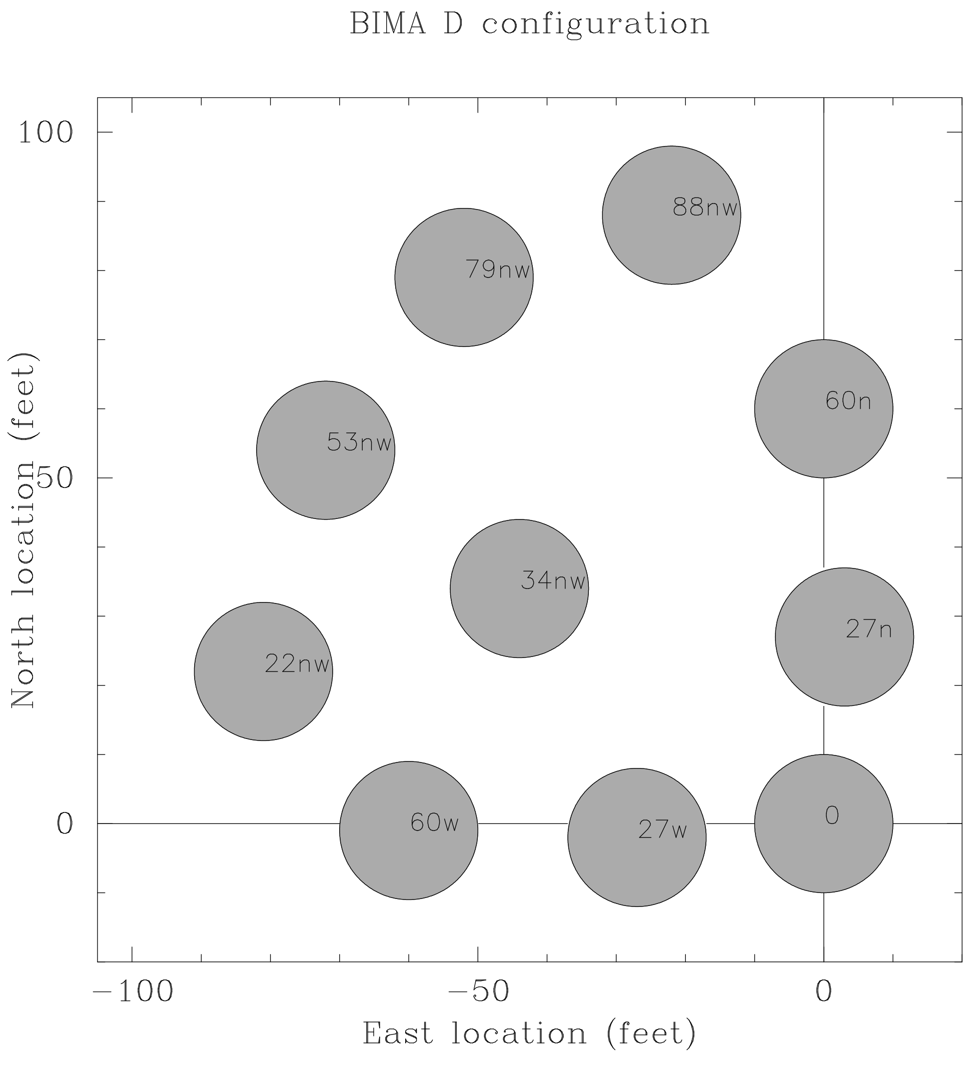

Figure 5: The 10 element BIMA D Array. The antenna locations on are a grid measured in feet (nsec).

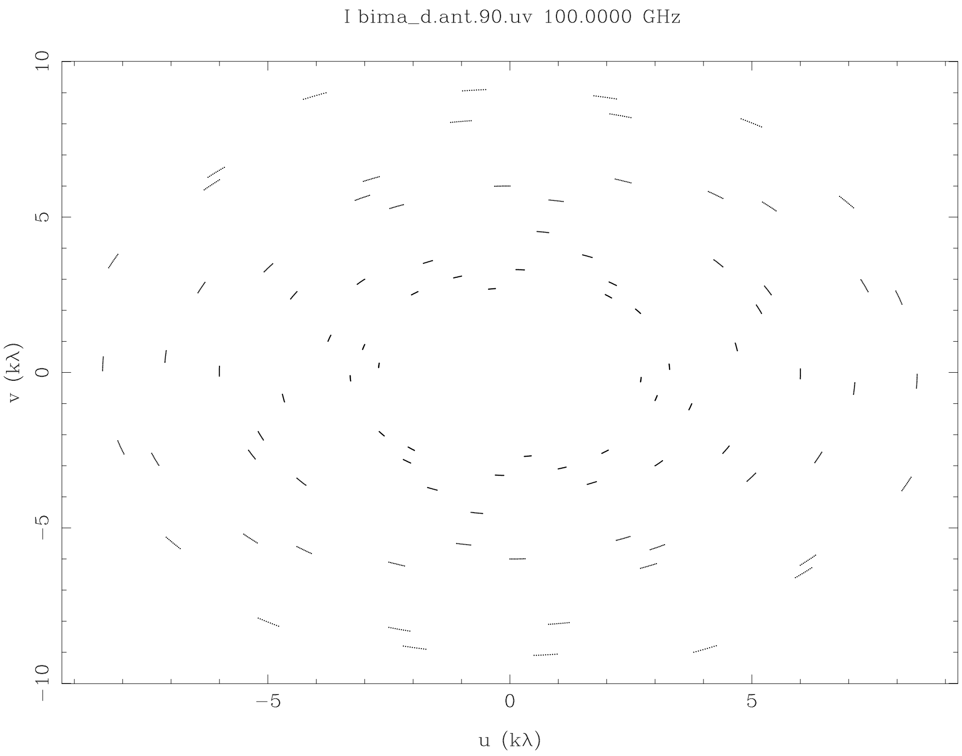

Figure 6: A snapshot set of visibilities for the BIMA D Array at a declination of 30^o. In this plot, $5.4k\lambda$ corresponds to a spacing of 16.2m, which would be the spacing of 12m antennas at a separation of 1.35. Including multiple pointings in the snapshot, the integration time for 6m antennas is 4 times longer than it is for the 12m antennas.

7 References

1. Sargent, A. I., and Welch, W. J. 1993, ARAA, 31. 297.
2. Perley, R. A., 1989, ASP Conference Series, no. 6, 287.
3. Ekers, R. D., and Rots, A. H., 1979, Proc. IAU Coll 49, Reidel, 61.
4. Cornwell, T. J., 1988, A &A, 202, 316.
5. Kogan, L. 1998, MMA Memo 217.